Inorganic Chemistry

Communication

pubs.acs.org/IC

Energy Upconversion in Lanthanide-Doped Core/Porous-Shell Nanoparticles

Yunxin Liu, Dingsheng Wang, Lingling Li, Qing Peng,* and Yadong Li*

Department of Chemistry, Tsinghua University, Beijing 100084, China

Supporting Information

ABSTRACT: Here, we report upconversion nanoparticles with a core/porous-shell structure in which bulk emission and nanoemission are simultaneously observed. The activated porous shell can efficiently tune the bulk emission but has negligible influence on the nanoemission.

Lanthanide-doped upconversion materials show unique photoluminescence of converting low-energy photons to higher-energy ones and can be efficiently excited by near-infrared (NIR) light. Because of superior photostability, deep tissue penetration of NIR excitation, and background-free imaging, lanthanide-doped upconversion nanoparticles (NPs) have recently received extensive and increasing attention in the field of biological labeling and imaging.[1] In comparison to upconversion bulk materials, upconversion nanocrystals have small particle size and high surface-to-volume ratio that supply the emission control with more tunable parameters. However, the remarkably lower emission efficiency relative to bulk materials hinders the development and application of upconversion nanocrystals. It is evidenced that the surface-quenching effect leads to the low luminescent efficiency of upconversion nanocrystals.[2] To overcome this drawback, a core/shell structure was developed to minimize the surface-quenching-induced emission losses.[3] Interestingly, the core/shell NPs show much stronger luminescence than bare core NPs. The upconversion emission from the cores with shell coating has a long fluorescent lifetime as a bulk material and is referred to as "bulk emission", while the one from bare cores with a shorter fluorescent lifetime due to surface defects is referred to as "nanoemission".[3] Here, we show a core/porous-shell (p-shell) structure in which bulk emission and nanoemission are simultaneously observed. The activated p-shell can efficiently tune the bulk emission but has negligible influence on the nanoemission.

$NaGdF_4$:Er^{3+}/$NaLnF_4$ (Ln = lanthanide) core/p-shell NPs were synthesized by thermal decomposition of trifluoroacetic salt.[4] The X-ray diffraction (Figure 1a) indicates that the synthesized $NaGdF_4$:Er^{3+} core NPs have hexagonal crystal structures and no precipitating phase or cubic transition phase was observed, demonstrating the successful substitution of Gd^{3+} by Yb^{3+} and Er^{3+} in C_{3h} sites. After fast growth with a p-shell of $NaYF_4$ (Figure 1b), $NaNdF_4$ (Figure 1c), and $NaYbF_4$ (Figure 1d), XRD patterns have no obvious change due to the overlap of XRD peaks of $NaLnF_4$ crystals.[5] The porous nature of these shells is confirmed by nitrogen physisorption (Figure S1 in the Supporting Information, SI). The average Barrett–Joyner–Halenda pore diameter is equal to 2.8, 2.7, and 3.0 nm for

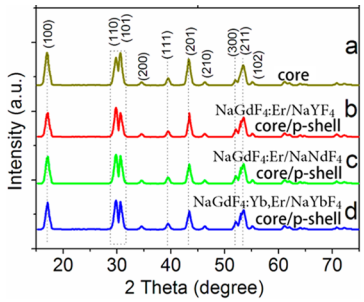

Figure 1. XRD spectra of (a) $NaGdF_4$:3%Er^{3+} core NPs, (b) $NaGdF_4$:3%Er^{3+}/$NaYF_4$, (c) $NaGdF_4$:3%Er^{3+}/$NaNdF_4$, and (d) $NaGdF_4$:3%Er^{3+}/$NaYbF_4$ core/p-shell NPs.

$NaNdF_4$, $NaYbF_4$, and $NaYF_4$ p-shells, respectively. The porous structures formed as a result of the growth process being controllably stopped before the formation of solid shells. From the transmission electron microscopy (TEM) image in Figure 2a, it is clear that $NaGdF_4$:Er^{3+} core NPs have capsule shape, uniform particle size (18 nm diameter), and a length-to-diameter ratio of 1.5. Figure 2b shows the TEM image of $NaGdF_4$:Er^{3+}/$NaYF_4$ core/p-shell NPs, in which the core and p-shell can be clearly distinguished because the p-shell has a lower volume density (see

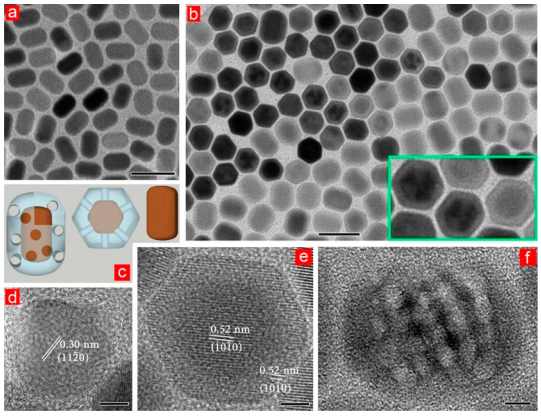

Figure 2. TEM images of (a) $NaGdF_4$:3%Er^{3+} core NPs and (b) $NaGdF_4$:3%Er^{3+}/$NaYF_4$ core/p-shell NPs. (c) Models for demonstrating the structures of $NaGdF_4$:3%Er^{3+} core NPs and $NaGdF_4$:3%Er^{3+}/$NaYF_4$ core/p-shell NPs. HRTEM images of (d) $NaGdF_4$:3%Er^{3+} core NPs and $NaGdF_4$:3%Er^{3+}/$NaYF_4$ core/p-shell NPs with (e) front and (f) side views, respectively. Scale bar: (a and b) 40 and (d–f) 5 nm.

Received: December 18, 2013
Published: March 27, 2014

   dx.doi.org/10.1021/ic403091w | *Inorg. Chem.* 2014, 53, 3257–3259

the models in Figure 2c), resulting in weaker contrast. The average thickness of the p-shell is equal to 4 nm. The single-crystal nature of the core nanocrystals was directly confirmed by the high-resolution TEM (HRTEM) image (Figure 2d), while the epitaxial growth characteristics of the p-shell could also be obviously observed from the HRTEM image (Figure 2e,f).

Alternatively, scanning TEM (STEM) images can also present the core/p-shell structures with surface information (Figure S2a in the SI). The electron energy loss spectroscopy (EELS) line scan conducted with STEM imaging (Figure S2b in the SI) on a $NaGdF_4:Er^{3+}/NaYF_4$ core/p-shell particle indicates an unusual elemental distribution that the troughs of Y elemental spectra from the $NaYF_4$ shell match with the crests of Gd elemental spectra from the $NaGdF_4$ core, and vice versa. It is easy to elucidate the EELS results that, for the pore position of the $NaYF_4$ shells, the $NaGdF_4$ cores were exposed so that strong EELS signals of the Gd element were detected (Gd crests). For the solid position of the $NaYF_4$ shells, the $NaGdF_4$ cores were screened by the shell so that weak EELS signals of the Gd element were detected (Gd troughs). This EELS result is obviously different from that in the core/solid-shell structure (Figure S3 in the SI) and provided direct evidence to the porosity of the shell in $NaGdF_4:Er^{3+}/NaYF_4$ core/p-shell NPs.

Fluorescence spectra of $NaGdF_4:Er^{3+}$ core NPs and $NaGdF_4:Er^{3+}/NaYF_4$ core/p-shell NPs were measured under an excitation of 980 nm NIR light and are shown in Figure 3a. It is

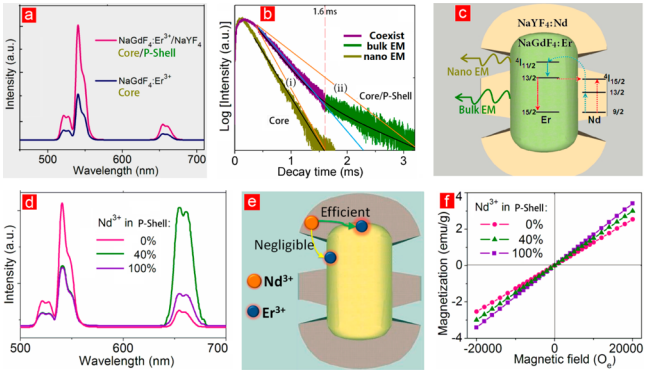

Figure 3. (a) Fluorescent spectra and (b) decay curve of the $^4S_{3/2}$ state (Er^{3+}) of $NaGdF_4:3\%Er^{3+}$ core and $NaGdF_4:3\%Er^{3+}/NaYF_4$ core/p-shell NPs. (c) Models for demonstrating the bulk emission and nanoemission and the energy transfer between Er^{3+} (in core) and Nd^{3+} (in shell). (d) Fluorescent spectra of $NaGdF_4:3\%Er^{3+}/NaYF_4:xNd^{3+}$ (x = 0, 40, and 100 mol %) core/p-shell NPs. (e) Models for demonstrating the energy-transfer processes from the shell to the naked surface or the coated surface of core NPs. (f) Magnetic field versus magnetization curves showing the paramagnetic nature of $NaGdF_4:3\%Er^{3+}/NaYF_4:Nd^{3+}$ core/p-shell NPs at room temperature and their dependences on the concentration of Nd^{3+} doping.

observed that the integral emission intensity of $NaGdF_4:Er^{3+}/NaYF_4$ core/p-shell NPs is more than 2 times that for $NaGdF_4:Er^{3+}$ core NPs because the surface defects of $NaGdF_4:Er^{3+}$ core NPs were considerably eliminated in the core/p-shell structures. Unsurprisingly, the lifetime of the $^4S_{3/2}$ energy level of Er^{3+} in $NaGdF_4:Er^{3+}/NaYF_4$ core/p-shell NPs is much longer than that in $NaGdF_4:Er^{3+}$ core NPs (Figure 3b).[3e] However, it should be noted that the fluorescent decay of $NaGdF_4:Er^{3+}/NaYF_4$ core/p-shell NPs occurs in two different stages (the decay rate before 1.6 ms is higher than that after 1.6 ms) and obviously distinguishes it from that of the core/shell structure (Figure S4 in the SI). For this phenomenon, it is suggested that the emission from both the naked surface and the surface with shell coating contributes to the fluorescence of core/p-shell NPs. As shown in Figure 3b, the decay curve of core/p-shell NPs can be divided into two parts, i and ii. Part i corresponds to the fluorescent decay of the naked surface (nanoemission), while part ii corresponds to the surface with shell coating (bulk emission; see Figure 3c). Then, it become clear that, for the first stage of the decay curve of core/p-shell NPs (before 1.6 ms), the fluorescence is actually composed of bulk emission and nanoemission (coexisting). At the second stage (after 1.6 ms), only bulk emission contributes to the fluorescence because nanoemission has completely vanished. The effective lifetime, τ_{eff}, was calculated based on the measured decay curves in Figures 3b and S4 in the SI by $\tau_{eff} = \int I(t)\,dt/I(0)$, where $I(t)$ is the fluorescence decay signal and $I(0)$ is the initial fluorescence intensity. The calculated effective lifetime of the $^4S_{3/2}$ state of the Er^{3+} ion is equal to 286, 417, and 515 μs for $NaGdF_4:Er^{3+}$ core, $NaGdF_4:Er^{3+}/NaYF_4$ core/p-shell, and $NaGdF_4:Er^{3+}/NaYF_4$ core/shell NPs, respectively. It is clear that the effective lifetime (417 μs) of the core/p-shell NPs is approximately equal to the average value (400.5 μs) of core and core/shell NPs. This means that bulk emission accounts for about half of the overall emission, while nanoemission takes the other half in these core/p-shell NPs (supplementary discussion in the SI; see part I for more information).

The active shell is more efficient than the inert shell for enhancing the upconversion luminescence.[6] Here, $NaYF_4$ p-shells were doped with Nd^{3+} ions to activate the shell and realize the energy transfer between the core and the shell,[7] of which the emission spectra are shown in Figure 3d. It is observed that the 542 nm green emission from the $^4S_{3/2}-^4I_{15/2}$ transition dominates the fluorescent spectra of the sample doped with 0 mol % Nd^{3+} in the p-shell, while the 654 nm red emission from the $^4F_{9/2}-^4I_{15/2}$ transition dominates the fluorescent spectra of the sample doped with 40 mol % Nd^{3+} in the p-shell. On the basis of the simplified energy level diagram in Figure 3c, it could be reasonably suggested that energy transfer between the Er^{3+} and Nd^{3+} ions occurred and led to the change of the electronic population in the $^4I_{11/2}$ and $^4I_{13/2}$ states of the Er^{3+} ion, resulting in the remarkable enhancement of the population probability of the $^4F_{9/2}$ state of Er^{3+} ions by the $^4I_{11/2}+^4F_{7/2}-2*^4F_{9/2}$ transitions.[8]

With a further increase in the Nd^{3+} content from 40 to 100 mol %, the intensity ratio of red to green emission decreases. On the basis of the model in Figure 3e, it is elucidated that Nd^{3+} ions in the p-shell can take an efficient energy exchange with Er^{3+} on the coated surfaces of core NPs but a negligible one with Er^{3+} on the naked surfaces of core NPs because of the surface defects. As a result, the doping of 40 mol % Nd^{3+} in the $NaYF_4$ p-shell only decreased the green portion from bulk emission but had no influence on the green portion from nanoemission. The further increase of the Nd^{3+} ion to 100 mol % in the p-shell also has no influence on the green portion from nanoemission. Emitter-doped $NaGdF_4$ (e.g., $NaGdF_4:Er^{3+}$) presents simultaneously fluorescent and paramagnetic properties because it contains paramagnetic ion Gd^{3+} and shows considerable paramagnetism even at room temperature. It is seen from Figure 3f that substitution of nonmagnetic ion Y^{3+} by paramagnetic ion Nd^{3+} in the p-shell also leads to enhancement of the paramagnetism of the core/p-shell NPs because of the increase of magnetization per unit volume.[8b,9]

The coexisting of bulk emission and nanoemission depends mainly on the core/p-shell structure. However, the shell

dx.doi.org/10.1021/ic403091w | Inorg. Chem. 2014, 53, 3257−3259

composition has considerable influence on its performance. The $NaYF_4$ p-shell is substituted with the $NaGdF_4$:Yb^{3+} p-shell to demonstrate this issue (Figure S5a,b in the SI). Green emission still dominates the overall fluorescence in $NaGdF_4$:Yb^{3+},Er^{3+}/$NaGdF_4$ core/p-shell NPs (Figure S5c in the SI). The doping of 20 mol % Yb^{3+} in the p-shell leads to remarkable enhancement of both green and red emission because the inert $NaGdF_4$ shell is activated by Yb^{3+} ions. Energy transfer between Er^{3+} ions (in the core) and Yb^{3+} ions (in the p-shell) is directly confirmed by the dependence of the emission intensity on the pump power (Figure S5d in the SI) that the electronic population of the $^4I_{11/2}$ state of Er^{3+} ions tends to saturate because of energy transfer from Yb^{3+} ions (in the p-shell) to Er^{3+} ions (in the core) under excitation of high pump power.

However, excess doping of Yb^{3+} in the p-shell, e.g., 100 mol % Yb^{3+} (see Figure S6 in the SI for the TEM image), decreases the total emission intensity because of the surface concentration quenching of Yb^{3+} ions.[10] It seems from the decay curves (Figure S5e in the SI) that bulk emission and nanoemission coexist only in the sample doped with 0 mol % Yb^{3+} in the p-shell. Actually, they coexist also in the samples doped with 20 and 100 mol % Yb^{3+}. However, for the sample doped with 20 mol % Yb^{3+} in the p-shell, the bulk emission dominates the overall fluorescence so that the corresponding decay curve shows the characteristics of bulk emission. For the $NaYbF_4$ p-shell (i.e., doped with 100 mol % Yb^{3+} in the p-shell), the nanoemission dominates the overall fluorescence so that the corresponding decay curve shows the characteristics of nanoemission. In addition, it is observed that the relative green emission from the sample with the $NaYbF_4$ p-shell is remarkably stronger than that from the one with the solid $NaYbF_4$ shell (Figure S7 in the SI), indicating the weak influence of the Yb^{3+} concentration quenching effect on the green nanoemission in $NaGdF_4$:Yb^{3+},Er^{3+}/$NaYbF_4$ core/p-shell NPs.

In conclusion, core/p-shell upconversion NPs were controllably synthesized, which shows simultaneously the bulk emission and nanoemission characteristics. The activated p-shell can efficiently tune the bulk emission but has negligible influence on the nanoemission. This directly confirms that efficient energy transfer relies on the intact crystal lattices and would be broken down by the surface defects on the NPs. In addition, this core/p-shell structure provides a platform for simultaneously researching the surface properties of the bare and coated NPs in a single system.

■ ASSOCIATED CONTENT

Ⓢ Supporting Information

Experimental section, Figures S1−S14, and a supplementary discussion. This material is available free of charge via the Internet at http://pubs.acs.org.

■ AUTHOR INFORMATION

Corresponding Authors

*E-mail: pengqing@mail.tsinghua.edu.cn.
*E-mail: ydli@mail.tsinghua.edu.cn.

Notes

The authors declare no competing financial interest.

■ ACKNOWLEDGMENTS

This work was supported by the State Key Project of Fundamental Research for Nanoscience and Nanotechnology (Grants 2011CB932401 and 2011CBA00500) and the National Natural Science Foundation of China (Grants 21171105, 21325101, 21231005, 21301058, and 21322107).

■ REFERENCES

(1) (a) Wang, L. Y.; Yan, R. X.; Huo, Z. Y.; Wang, L.; Zeng, J. H.; Bao, J.; Wang, X.; Peng, Q.; Li, Y. D. *Angew. Chem., Int. Ed.* **2005**, *44*, 6054−6057. (b) Chatterjee, D. K.; Rufaihah, A. J.; Zhang, Y. *Biomaterials* **2008**, *29*, 937−943. (c) Hilderbrand, S. A.; Shao, F.; Salthouse, C.; Mahmood, U.; Weissleder, R. *Chem. Commun.* **2009**, 4188−4190. (d) Mader, H. S.; Kele, P.; Saleh, S. M.; Wolfbeis, O. S. *Curr. Opin. Chem. Biol.* **2010**, *14*, 582−596. (e) Liu, Q.; Sun, Y.; Yang, T.; Feng, W.; Li, C.; Li, F. *J. Am. Chem. Soc.* **2011**, *133*, 17122−17125. (f) Zhan, Q.; Qian, J.; Liang, H.; Somesfalean, G.; Wang, D.; He, S.; Zhang, Z. G.; Andersson-Engels, S. *ACS Nano* **2011**, *5*, 3744−3757. (g) Wang, F.; Banerjee, D.; Liu, Y. S.; Chen, X. Y.; Liu, X. G. *Analyst* **2010**, *135*, 1839−1854. (h) Zhou, J. C.; Yang, Z. L.; Dong, W.; Tang, R. J.; Sun, L. D.; Yan, C. H. *Biomaterials* **2011**, *32*, 9059−9067. (i) Kumar, R.; Nyk, M.; Ohulchanskyy, T. Y.; Flask, C. A.; Prasad, P. N. *Adv. Funct. Mater.* **2009**, *19*, 853−859. (j) Chen, G.; Shen, J.; Ohulchanskyy, T. Y.; Patel, N. J.; Kutikov, A.; Li, Z.; Song, J.; Pandey, R. K.; Ågren, H.; Prasad, P. N.; Han, G. *ACS Nano* **2012**, *6*, 8280−8287. (k) Pichaandi, J.; Boyer, J. C.; Delaney, K. R.; Van Veggel, F. C. *J. Phys. Chem. C* **2011**, *115*, 19054−19064. (l) Chen, G.; Ohulchanskyy, T. Y.; Liu, S.; Law, W. C.; Wu, F.; Swihart, M. T.; Ågren, H.; Prasad, P. N. *ACS Nano* **2012**, *6*, 2969−2977. (m) Zeng, S.; Tsang, M. K.; Chan, C. F.; Wong, K. L.; Hao, J. *Biomaterials* **2012**, *33*, 9232−9238. (n) Nyk, M.; Kumar, R.; Ohulchanskyy, T. Y.; Bergey, E. J.; Prasad, P. N. *Nano Lett.* **2008**, *8*, 3834−3838. (o) Xie, X. J.; Gao, N. Y.; Deng, R. R.; Sun, Q. Q.; Xu, H.; Liu, X. G. *J. Am. Chem. Soc.* **2013**, *135*, 12608−12611. (p) Cheng, L.; Yang, K.; Zhang, S.; Shao, M.; Lee, S.; Liu, Z. *Nano Res.* **2010**, *3*, 722−732. (q) Yu, X.; Li, M.; Xie, M.; Chen, L.; Li, Y.; Wang, Q. *Nano Res.* **2010**, *3*, 51−60.

(2) (a) Song, H.; Sun, B.; Wang, T.; Lu, S.; Yang, L.; Chen, B.; Wang, X.; Kong, X. *Solid State Commun.* **2004**, *132*, 409−413. (b) Wang, F.; Wang, J.; Liu, X. G. *Angew. Chem.* **2010**, *122*, 7618−7622.

(3) (a) Yi, G. S.; Chow, G. M. *Chem. Mater.* **2007**, *19*, 341−343. (b) Qian, H. S.; Zhang, Y. *Langmuir* **2008**, *24*, 12123−12125. (c) Abel, K. A.; Boyer, J. C.; van Veggel, F. C. J. M. *J. Am. Chem. Soc.* **2009**, *131*, 14644−14645. (d) Boyer, J. C.; Gagnon, J.; Cuccia, L. A.; Capobianco, J. A. *Chem. Mater.* **2007**, *19*, 3358−3360. (e) Wang, F.; Deng, R.; Wang, J.; Wang, Q.; Han, Y.; Zhu, H.; Chen, X.; Liu, X. *Nat. Mater.* **2011**, *10*, 968−973. (f) Dong, C.; Korinek, A.; Blasiak, B.; Tomanek, B.; van Veggel, F. C. *Chem. Mater.* **2012**, *24*, 1297−1305. (g) Xin, F.; Zhao, S.; Huang, L.; Deng, D.; Jia, G.; Wang, H.; Xu, S. *Mater. Lett.* **2012**, *78*, 75−77. (h) Zhang, C.; Lee, J. Y. *ACS Nano* **2013**, *7*, 4393−4402. (i) Sun, L.; Zhu, G.; Zhao, Y.; Yan, X.; Mou, S.; Dovichi, N. J. *Angew. Chem., Int. Ed.* **2013**, *125*, 13661−13665.

(4) Boyer, J. C.; Vetrone, F.; Cuccia, L. A.; Capobianco, J. A. *J. Am. Chem. Soc.* **2006**, *128*, 7444−7445.

(5) Abel, K. A.; Boyer, J. C.; Andrei, C. M.; van Veggel, F. C. *J. Phys. Chem. Lett.* **2011**, *2*, 185−189.

(6) Vetrone, F.; Naccache, R.; Mahalingam, V.; Morgan, C. G.; Capobianco, J. A. *Adv. Funct. Mater.* **2009**, *19*, 2924−2929.

(7) (a) Zhu, H.; Chen, X.; Hung, T. F.; Wang, B. L.; Zhu, G. Y.; Yu, S. F.; Wang, F. *Angew. Chem., Int. Ed.* **2013**, *52*, 13419−13423. (b) Wang, Y.; Liu, G.; Sun, L.; Xiao, J.; Zhou, J.; Yan, C. *ACS Nano* **2013**, *7*, 7200−7206.

(8) (a) Wang, F.; Han, Y.; Lim, C. S.; Lu, Y.; Wang, J.; Xu, J.; Chen, H.; Zhang, C.; Hong, M.; Liu, X. *Nature* **2010**, *463*, 1061−1065. (b) Liu, Y.; Wang, D.; Shi, J.; Peng, Q.; Li, Y. *Angew. Chem., Int. Ed.* **2013**, *52*, 4366−4369.

(9) (a) Zhou, J.; Sun, Y.; Du, X.; Xiong, L.; Hu, H.; Li, F. *Biomaterials* **2010**, *31*, 3287−3295. (b) Liu, Y.; Tu, D.; Zhu, H.; Li, R.; Luo, W.; Chen, X. *Adv. Mater.* **2010**, *22*, 3266−3271.

(10) Wu, F.; Liu, X.; Kong, X.; Zhang, Y.; Tu, L.; Liu, K.; Song, S.; Zhang, H. *Appl. Phys. Lett.* **2013**, *102*, 243104.